Daytime Sky Brightness Measurements and Comparison to Analytical Models

Vincent Vella
L3Harris Technologies
Jacob Brazeau
L3Harris Technologies

ABSTRACT

The daytime sky brightness is measured in multiple bands over the full celestial sphere at multiple times in order to establish baseline nominal conditions for radiometric link budget estimates as well as to compare spectral responses against theoretical black body estimates. The magnitude and frequency of scattering and aerosol impacts causing variances from benign low scattering profiles are compared against various common MODTRAN profiles with an investigation into the measurements' correlation to the models' outputs.

BACKGROUND

Sky brightness is an important limiting factor for daytime space domain awareness (SDA.) As is evident from the limiting value of the Charge Coupled Device (CCD) Signal-to-Noise-Ratio (SNR) equation, the large daytime background flux densities will cause the following limiting behavior: $SNR \rightarrow \frac{\dot{S}}{\sqrt{2\dot{B}}}$ [1]. Here, $\dot{S}$ is the signal flux density from a Resident Space Object (RSO) and $\dot{B}$ is the background signal flux density, respectively. Both are a function of the band-pass, bandwidth, viewing angles to sources, and directional radiances due to its manner of scattering. As can be seen by this simple limit, only a change in RSO attributes, increase in flux densities via larger apertures, or a relative reduction in background flux can impact the SNRs. generally the RSO attributes are not pursuant to ground sensor control, and larger apertures are costly and subject to diminishing returns when in the presence of strong scattering, leaving a reduction in background flux the last parameter which can be varied. Background flux reduction is achieved either through vignetting with the unfortunate loss in signal flux, or through judicious selection of quality geographical locations and operating band-passes which feature less bright skies due to an absence of atmospheric scattering at those wavelengths. This last point was the inspiration for our investigations.

To gain an understanding of the variances between local conditions, time of day and look angles, the sky was scanned with a custom-built photo-diode sensor system. These featured a mix of commercial-off-the-shelf (COTS) sensors and custom integrated photodiodes based on Indium Gallium Arsenide (InGaAs) Photo-injection (PIN) material. The system featured of the following bands, which will later be formally defined, and they are listed with the equipment which sensed it:

a) Johnson V-Band via the "Unihedron *Sky Quality Meter Low-Look Angle Ethernet*" (SQM-LE)
b) "1.39μm-Band" via the "Marktech *MTPD-1346-100*" InGaAs PIN Photodiode
c) "1.89μm-Band" via the "Marktech *MTPD-2600-100*" InGaAs PIN Photodiode

d) "1.39µm-Band Check" via the "Marktech *MTD6013D3-PD" InGaAs PIN* Photodiode

The bands as defined above are formally plotted in **Error! Reference source not found.**, along with the representative "Top-Hat" equivalents which were used for integrated radiance inputs for "Moderate resolution atmospheric Transmission" (MODTRAN) simulations. For V-Band, published values were used [2], and for the other filters the Quantum Efficiency and Responsivities were normalized to percentage of maximum. Then, each stepwise value was integrated step-wise against the total integrated area. We observed that Band 4, "1.39µm-Band Check", did not produce consistent results over multiple data collection runs nor within single runs. We propose that the inconsistent results in Band 4 were on account of the hemispherical lens used in that photodiode, whereas the other photodiodes each featured flat-window housings, which led to differences in underlying directional aperture. Regardless, this band's results were discarded and will not be presented in the remainder of the paper.

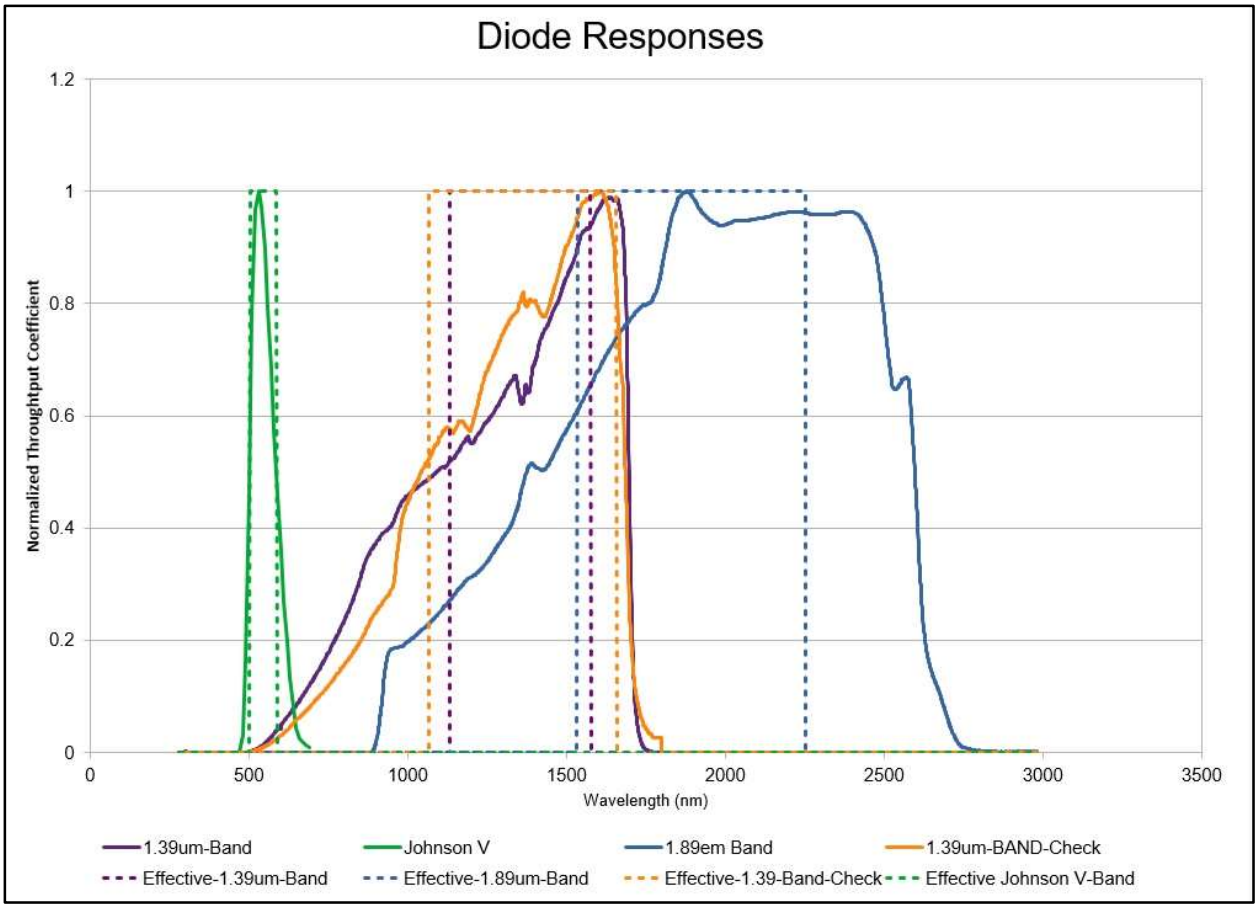

Figure 1: Filter Response

Differences in measurements across the bands and in different viewing directions for the remaining bands were observed. These did not always result in a symmetrical pattern across the separate bands nor were they always consistently offset across each band. These differences would normally be expected from the changes in the solar black-body spectrum which is illuminating

the atmosphere, which would then be scattered by the constituents of the atmosphere as well as strong interaction with the molecules contained therein, so the measurements are suggestive of a varied degree of scattering in the different bands in the various directions. Comparison of the results obtained over three different days were made with predictions based on the analytical simulations provided by MODTRAN to determine the feasibility in use of simulations in SDA validation and verification. A short description of the method of measurement and comparisons will be outlined prior to report of the measurements.

The primary components of the system hosting these photodiodes included an astronomical positioning mount calibrated to within 1 degree pointing area, the sensing diodes housing, a programmable gain low-noise amplified analog-to-digital-convertor (ADC), and a control computer with SW for conversion. The housing were cylindrical plastic shrouds cut to a length to ensure a ~15º full-width-half-max (FWHM) field stop, and the amplifier/ADC combo was based on the Ada-Fruit ADS1015 module. The mount control and ADC converted values were parsed via a Raspberry Pi 4.

Finally, after data acquisition, MODTRAN simulations were compared with the measurements. The simulations were obtained via the online tool "Coupled Ocean Atmospheric Radiative Transfer" (COART) [3], [4]. This tool allows for the selection of atmospheric models, aerosol characteristics, time and locations, and degree of coupling to surface area. The parameters used are explained in a later section. We also elected to use our effective-band integrated radiance outputs using the previously plotted values, which we then configured to span a full simulated celestial sphere. Although we were measuring directional isolation (irradiance), the radiance values were sufficient to obtain relative flux densities. These corresponded to the measured irradiance and the outputs of which were much more convenient for plotting and qualitative model comparisons. Strict comparisons to absolute values would require a translation between the radiances and different diode responsivities. Our V-Band data was correctly calibrated using a "Thousand Oaks Type II" solar film on the Sky Quality Meter. The differences between "with film" during day, and "without film" during a following night during a week of high-pressure steady weather conditions were then used to determine an offset to convert the filtered daytime SQM-LE V-Band readings to correct notional values. The two types of short-wave infrared (SWIR) values, i.e. our measured ADC counts and the simulated radiances, were both offset to match a similar colormap over 3 magnitudes of brightness variation. Their absolute values are not reported (nor meaningful as the diode-responses were not correlated against standard bands for our purposes.)

DESCRIPTION OF DAYTIME BRIGHTNESS MEASUREMENTS

The daytime brightness results demonstrate good qualitative agreement with expectations, showing a nominal 2-3 magnitude change across the sky in each band. We elected to clip the measurements which would include the Sun to this maximum 3 magnitudes above the minima. The step sizes for both measurements and simulations are every 10 degrees from 5 (Zenith) to 85 deg (Near Horizon) in elevation, and 9 degrees each in Azimuth, scaled as COS (Elevation). Thus, giving our field of view, we are oversampling with respect to our aperture. However, the broad beamwidth of the aperture implies we are also still admitting bright light sources which are far off-axes. This has the effect of broadening our maps artificially. This broadening has not been

normalized as the lower resolution maps were still sufficient for our needs. The pointing accuracy is expected to be within 1º. We do not account for sidereal rotation over the approximately 1 hour required to scan the sky. We also do not account for the underlying aperture/angle of incidence beam-directivity as the diodes are looking out of their shrouds. Finally, we acknowledge the shrouds themselves exhibit an unknown but noticeable reflectance in the visual band and are assumed to behave similarly in the short-wave infrared. Such behavior will mimic atmospheric scattering and contaminate the scattering measurements except over broad spatial extents. We nevertheless ignore these factors and base our qualitative comparison analysis between measurements and simulation accordingly. To help demonstrate the comparisons, we linearly interpolated between the sparsely sampled measurements and simulations; in so doing we did not attempt apply an aperture kernel for more realistic interpolation. As a result, the values presented are assumed consistent relative to each other but expect the comparisons themselves to be of course fidelity. Admittedly the results also include a good deal of bias offset and regions of bright sources are artificially broadened. That is, the results have not been normalized to account for extended sources continued within the large beamwidth nor for translation from the 30º solid angle to a magnitude per square arcsecond. Despite these limitations, the results were sufficient both to draw some important conclusions and for use in comparison against the MODTRAN outputs which will be presented in the following section.

QUALITATIVE COMPARISON WITH ANALYTICAL MODELS

The results of the measurements are presented for two separate days and locations. The first location was day-of-year (DOY) 059 near Longmont, Colorado, USA. Local conditions were clear with little to no breeze and local time was about 19:00 UTC. Given the time of year we elected to utilize “Mid-Latitude-Winter” as the underlying atmospheric models in all but the simulations except the nominal case. The second location and set of measurements were DOY 148 near Colorado Springs, CO, USA. Local conditions were again clear, little to no breeze, and the data collection was near 19:55 UTC. Given the time of year for these measurements we elected to utilize “Mid-Latitude-Summer” as the underlying atmospheric models in all of the simulations but the nominal case. In both cases, “Nominal” models utilized the standard US62 Atmospheric model with no local or stratospheric scattering. A composite figure for each day and each of the three bands (V, 1.39, 189) are presented in
Figure 2: DOY 059 Measured V-Band,
Figure 3: DOY 059 Measured "1.35μm-Band", Figure 4: DOY 059 Measured "1.89μm-Band”, Figure 5: DOY 148 Measured V-Band, Figure 6: DOY 148 "1.39μm-Band", and Figure 7: DOY 148 "1.89μm-Band", respectively, and each present the measurements, the nominal simulation, and then 5 other configurations used as a representative sampling of different aerosol conditions. All of these configurations are:

- NOM: US62 Atmosphere, No Mixed Layer Aerosols, No Tropospheric Aerosols
- CFG1: MLS (DOY 148) or MLW (DOY 059) Atmosphere, “Rural” Mixed Layer Aerosols, “Background” Tropospheric Aerosols
- CFG2: MLS (DOY 148) or MLW (DOY 059) Atmosphere, “Urban” Mixed Layer Aerosols, “Background” Tropospheric Aerosols

- CFG3: MLS (DOY 148) or MLW (DOY 059) Atmosphere, “OPAC Desert” Mixed Layer Aerosols, “Background” Tropospheric Aerosols
- CFG4: MLS (DOY 148) or MLW (DOY 059) Atmosphere, “OPAC Continental Polluted” Mixed Layer Aerosols, “Extreme Volcanic” Tropospheric Aerosols
- CFG5: MLS (DOY 148) or MLW (DOY 059) Atmosphere, “OPAC Continental Average” Mixed Layer Aerosols, “Moderate Volcanic” Tropospheric Aerosols

One additional factor was utilized in these simulations. The COART simulations contain the ability to couple the simulation with a reflective surface such as the ocean. We noted two related factors: first, the ideal location for a daytime sensor would be near a body of water to benefit from the lake-effect on calming steadiness. Secondly, the results from the coupled simulations featured far more realistic variances than the non-coupled outputs. Therefore, in all cases a 5m ocean surface depth was applied.

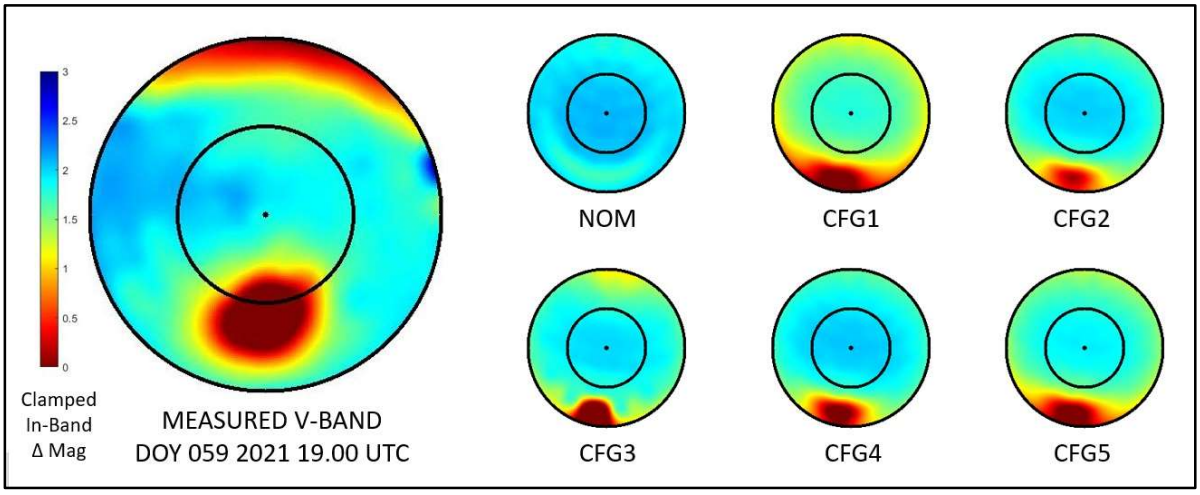

Figure 2: DOY 059 Measured V-Band

For the DOY059 Visual data, we found best simulation qualitative agreements of: CFG3, 4, 5, 2, 1, and NOM, in that order.

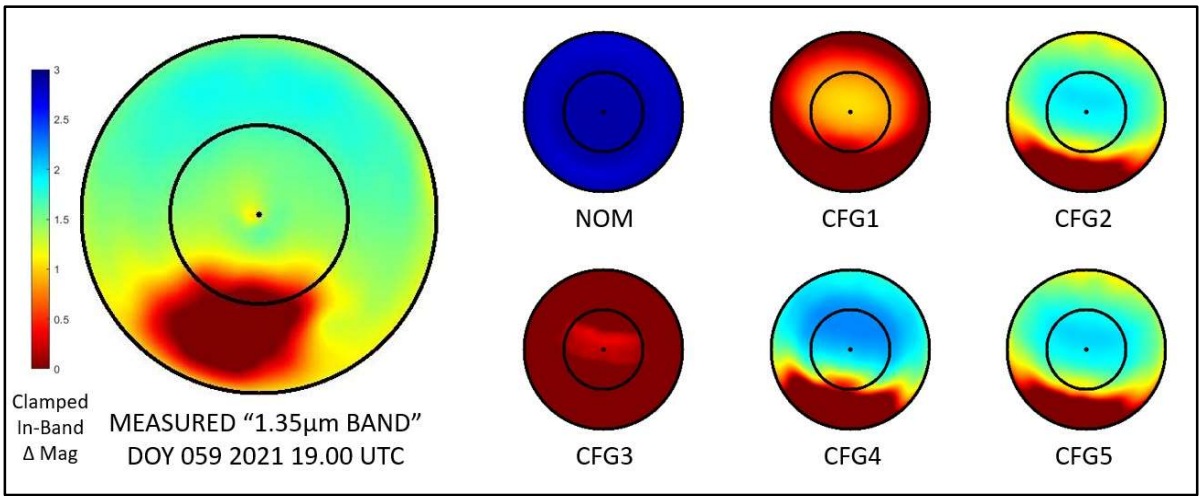

Figure 3: DOY 059 Measured "1.35µm-Band"

For the DOY059 1.39µm data, we found best simulation qualitative agreements of: CFG4, 2, 5, 1, 3, and NOM, in that order.

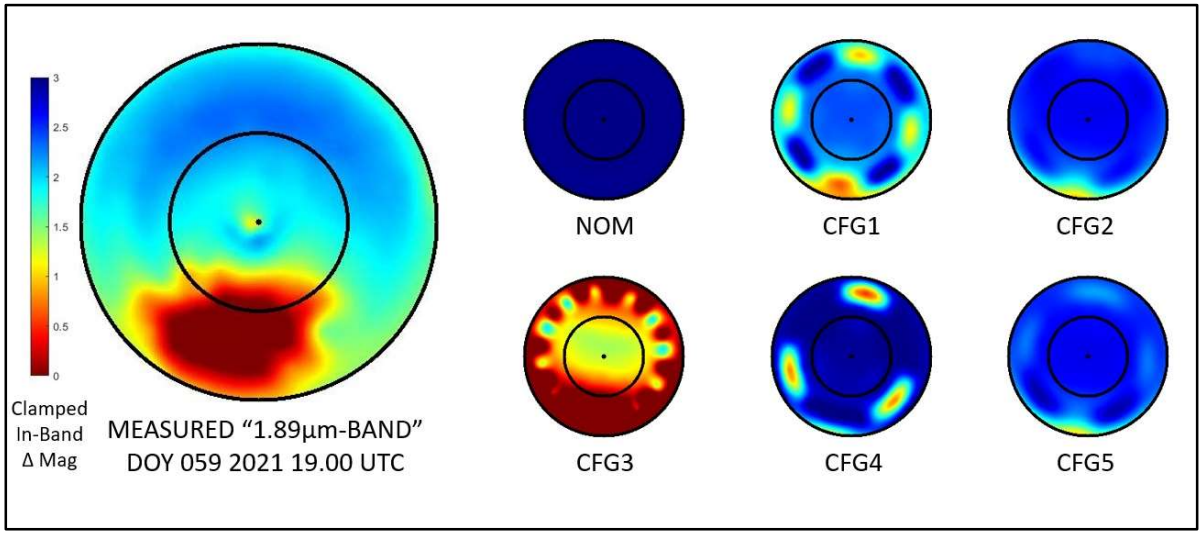

Figure 4: DOY 059 Measured "1.89µm-Band"

For the DOY059 1.89µm data, we found best simulation qualitative agreements of: CFG2, 4, 5, 1, 3, and NOM, in that order.

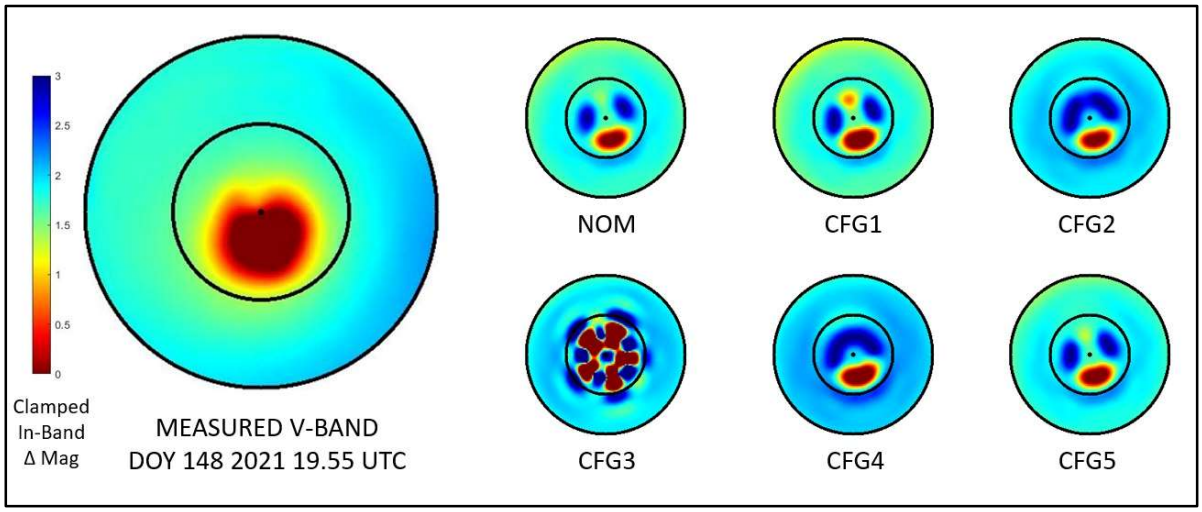

Figure 5: DOY 148 Measured V-Band

For the DOY148 visual data, we found best simulation qualitative agreements of: NOM, CFG2, 4, 1, 5, and 3, in that order.

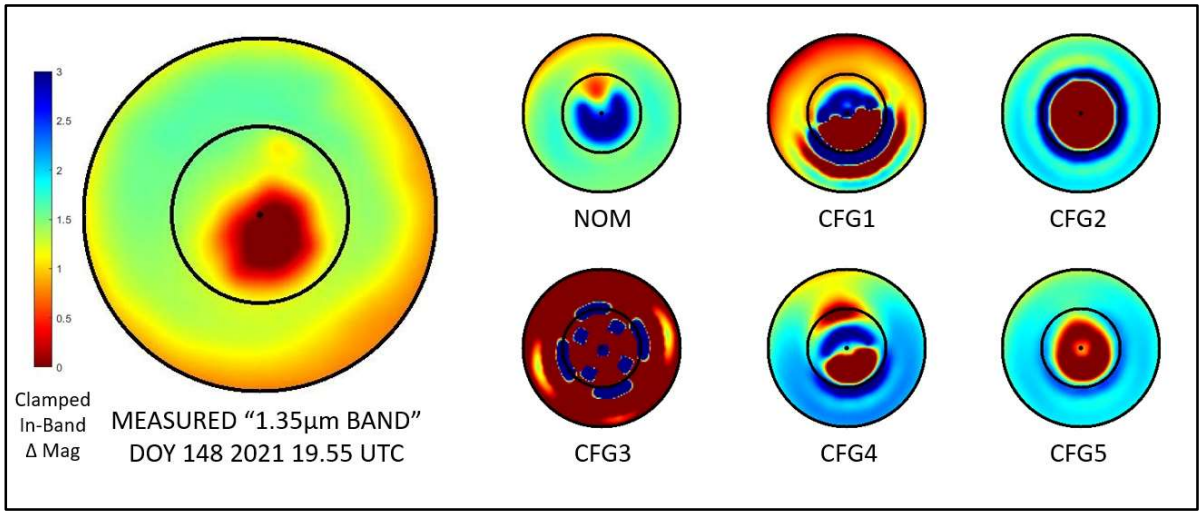

Figure 6: DOY 148 "1.39µm-Band"

For the DOY148 1.39µm data, we found best simulation qualitative agreements of: NOM, CFG4, 2, 5, 3, and 1, in that order.

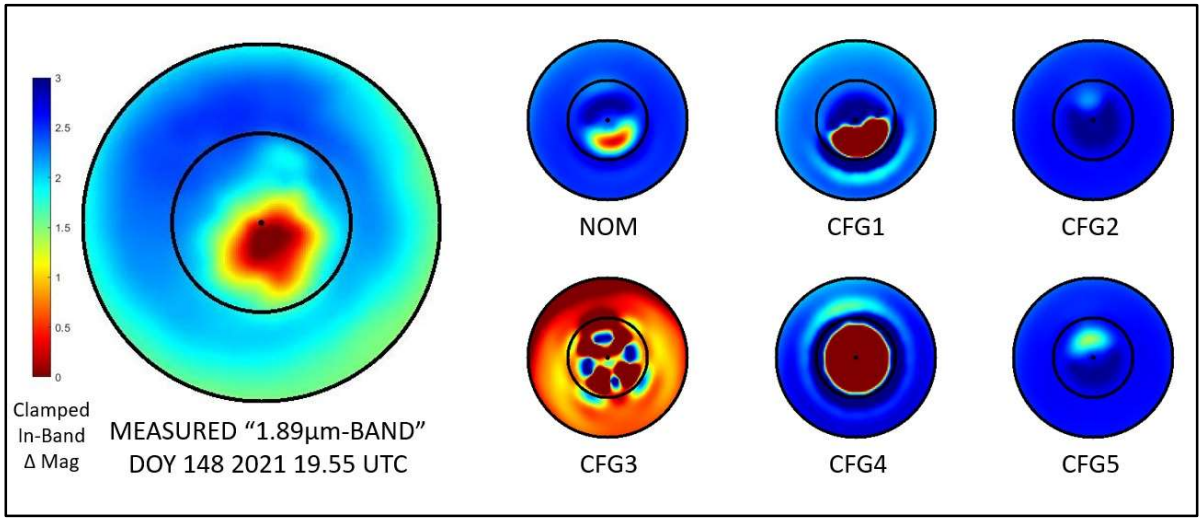

Figure 7: DOY 148 "1.89µm-Band"

For the DOY148 1.89µm data, we found best simulation qualitative agreements of: CFG1, NOM, 4, 2, 1, and 3, in that order.

In summary, we notice in most cases the non-aerosol simulations do not well predict the measurements. In addition, the optimal configurations which do fit the measurement predictions are not consistent across the bands nor the days of year. The variances all suggest 3 magnitudes or more of variation across significant portions of the sky is the rule rather than the expectation. These results lend support to a stochastic approach where atmospheric parameters are carefully tuned to match the site based on real world measurements or aggregate averages.

IMPLICATIONS FOR SPACE DOMAIN AWARENESS

We note the three-fold or greater variance within the results. Considering the limiting SNR value of $S/\sqrt{2B}$, we see that this corresponds to at least a factor of $\sqrt{10^{0.4*3}} \sim 2.5$ magnitude reduction in detection at worst. A similar relationship can be seen in a telescope aperture which is varied due to the r^2 surface area with respect to increase in radius. This means a mirror, all other factors being equal, would need to an increase the same $\sqrt{10^{0.4*2}} = 4$ times larger to compensate. Various sources have demonstrated that the cost of such elements is exponential with size. Thus, there is a huge cost-to-performance gain to be had in both selection of optimal sites, and tailoring site operations to take advantage of current changing conditions. We also note that much smaller (and therefore more amenable to being portable) sensors could, if deployed to ideal sites, compete with much longer fix installations under adverse conditions. The physical limitations of the smaller aperture would never compete with the larger ones in an optimal location; however, we suggest a combination of the two wherein the smaller apertures augment the more established larger ones. We propose that this could possibly be a more effective combination if the fixed

installation is in a non-ideal location where it needs to contend with adverse conditions for a significant amount of time. The key conclusion here is that site selection and tailoring operations to meet them is likely to equal or surpass in terms of cost/performance balance any other SDA system element.

SUMMARY

The daytime sky brightness was measured in sub-bands across the Visual and SWIR spectrum. Look-angle dependent variances of over three magnitudes within each band were observed. The results were compared with six separate simulated atmospheric and aerosol scattering models within each band. Each set of simulations had results which more closely aligned with the measurements than the other simulations within that set. However, we note very little consistency or correlation between the best match across the bands, and large variances between day of year and best fits. We compare the variances with impacts on noise-limited SDA signal-to-noise ratios (SNRs) and come to the following strong conclusions. Either a stochastic combination of a large number of simulations should be used to tune the numerical models against a specific geographical site profile and/or real measurements from the site are recommended. This is preferred to attempting to select one of the preexisting macroscopic numerical models and applying that single model to a site. We note that the results favor a strategy of selection of the optimal site for fixed large-aperture sensors along with an emphasis on agility and portability for smaller sensors which could optimally relocate to the best site under changing conditions. We thus find that site selection and system optimization to take best advantage of the site is one of the most critical factors in an SDA system. The authors would like to gratefully acknowledge the Space and Missile Center (SMC) Directorate of Special Projects (Dir-SP) efforts in support of Space Surveillance System (SSN) sustainment and associated conversations with the SMC team thereof as inspiration for this study.

1. REFERENCES

[1] Binney, James, Merrifield, Michael. *Galatic Astronomy*, Princeton University Press, 1998.
[2] Bessell, M.S. UBVRI passbands, Astronomical Society of the Pacific, v102:1181-1199, 1990.
[3] Jin, Z., at al. *Analytical solution of radiative transfer ion the coupled atmosphere-ocean system with a rough surface.* Appl. Opt. v45:7443-7455, 2006
[4] Jin, Z. et al. *Coupled Ocean and Atmosphere Radiative Transfer (COART)* Website, https://cloudsgate2.larc.nasa.jov/jion/coart.html. Retrieved May 29, 2021.